Catalysis Today 180 (2012) 51–58

Contents lists available at ScienceDirect

Catalysis Today

journal homepage: www.elsevier.com/locate/cattod

Oxidative dehydrogenation of ethane over NiO–CeO_2 mixed oxides catalysts

Benjamín Solsona [b,*], Patricia Concepción [a], Selene Hernández [a], Benjamin Demicol [b], José M. López Nieto [a,*]

[a] Instituto de Tecnología Química, UPV-CSIC, Campus de la Universidad Politécnica de Valencia, Av. Naranjos s/n, 46022 Valencia, Spain
[b] Departamento de Ingeniería Química, Universitat de Valencia, c/Dr. Moliner 50, 46100 Burjassot, Spain

ARTICLE INFO

Article history:
Received 11 January 2011
Received in revised form 27 March 2011
Accepted 28 March 2011
Available online 13 May 2011

Keywords:
Oxidative dehydrogenation of ethane
Ethylene
Cerium oxide
Nickel oxide
Catalyst characterization (XPS, TPR, XRD, Raman, FTIR of adsorbed CO, oxygen isotopic-exchange)

ABSTRACT

In this paper we present the synthesis, characterization and catalytic behaviour in the oxidative dehydrogenation of ethane of NiO–CeO_2 mixed oxides. The addition of cerium oxide to NiO strongly modifies its catalytic performance, although the changes in the catalytic behaviour depend on the catalyst composition. The incorporation of low amounts of cerium oxide to NiO multiplies the productivity to ethylene in the oxidative dehydrogenation of ethane by a factor of ca. 7, which is the result of an increase in both catalytic activity and selectivity to ethylene. The enhanced activity has been related to the remarkable increase of the surface area of catalyst and the low crystal sizes of NiO that takes place when a tiny amount of cerium oxide is incorporated to the NiO. The higher selectivity to ethylene has been related to the modification of the nature of Ni–O species, which implies a lower production of carbon oxides. On the other hand, high activity and selectivity is also observed over catalysts rich in cerium (with Ni/Ce ratios between 0.2 and 3). In this case, a different mechanism can be proposed in which the high capacity of CeO_2 to bomb oxygen from bulk to surface and the partial formation of NiO and $Ce_{1-x}Ni_xO_2$ facilitates a faster reoxidation of active Ni-sites by a synergic effect improving catalytic activity.

1. Introduction

Ethylene is widely used as a chemical feedstock for numerous processes and products of high economic value, thus dictating ethylene's high price relative to ethane. In fact ethylene is the main building block in petrochemistry [1,2].

The catalytic oxidative dehydrogenation (ODH) of ethane could be an interesting alternative to the current industrial processes (steam cracking or as a by-product in catalytic cracking) for the production of ethylene [3,4] since is thermodynamically favoured at low temperatures and coke is not formed. For this process the two most important catalytic systems are (i) MoVTe(Sb)NbO catalysts [5,6] and (ii) NiO-based mixed oxide catalysts [7–14].

It has been reported in the literature that nickel oxide alone acts with a high activity but a very low selectivity to ethylene, whereas when another metals, such as niobium [9,10], tungsten [11] or non-reducible elements with high valence [12], are added to the NiO the selectivity to ethylene remarkably increases.

One of the main downsides of the active and selective catalytic systems studied up to date is the relatively low productivity to ethylene that has been obtained. Thus, apart from high selectivity towards ethylene, productivities higher than 1.0 $kg_{C_2H_4}\ kg_{cat}^{-1}\ h^{-1}$, are required to compete with the steam-cracking process [15].

Therefore, as NiO is a relatively active catalyst it would be interesting to enhance its reactivity improving at the same time the selectivity to ethylene. We have thought that the addition of cerium to NiO could enhance the catalytic activity due to:

(i) the presence of CeO_2 could favour the formation of NiO particles with smaller crystal sizes and higher surface areas (and consequently increase the catalytic activity) than the corresponding pure NiO,
(ii) cerium oxide (CeO_2) is recognised as having versatile properties as a catalyst and presents the ability to transport oxygen in combination with the ability to cycle easily between reduced and oxidized states (i.e. Ce^{3+}–Ce^{4+}) [16–18] then increasing the reaction rate for reactions which take place through redox mechanisms.

Ni–Ce–O catalysts have been reported to be efficient for the oxidative dehydrogenation of propane into propylene [19–21] although all these studies have been conducted using high Ce-loadings. Liu et al. [21] obtained high yields to propylene during the ODH of propane over Ni–Ce–O catalysts proposing that high dispersion of nickel oxide is required in order to obtain more active and selective catalysts.

* Corresponding authors. Fax: +34 966877809.
E-mail addresses: benjamin.solsona@uv.es (B. Solsona), jmlopez@itq.upv.es (J.M.L. Nieto).

0920-5861/$ – see front matter © 2011 Elsevier B.V. All rights reserved.
doi:10.1016/j.cattod.2011.03.056

In the present work it has been studied the oxidative dehydrogenation of ethane on Ni–Ce–O catalysts (for the first time to the best of our knowledge) paying attention to compositions very rich in Ni, demonstrating the promoter effect of ceria on the NiO base catalyst. It has been demonstrated that the addition of cerium (even just a tiny amount of cerium Ce/Ni = 0.02 at. ratio) highly increases the productivity towards ethylene as a result of an improvement in both the catalytic activity and the selectivity to ethylene. In fact, these Ni–Ce–O catalysts can selectively activate an alkane as relatively inert as ethylene is at a reaction temperature of only 250 °C.

2. Experimental

2.1. Catalyst preparation

Ni–Ce–O mixed metal oxides catalysts were prepared through the evaporation at 60 °C of a stirred ethanol solution of nickel nitrate ($Ni(NO_3)_2{\cdot}6H_2O$ from Sigma–Aldrich) and cerium nitrate ($Ce(NO_3)_3{\cdot}6H_2O$ from Sigma–Aldrich). Oxalic acid was added to the solution with an oxalic acid/(Ni + Ce) ratio (molar) in all cases of 1 for consistency. The solids were dried overnight at 120 °C, and finally calcined in static air for 2 h at 500 °C.

The catalysts will be named as NiCe-*x*, where *x* is the Ni/Ce ratio in the synthesis gel.

2.2. Catalysts characterization

Catalyst surface areas were determined by multi-point N_2 adsorption at −196 °C. The data was treated in accordance with the BET method.

Powder X-ray diffraction was used to identify the crystalline phases present in the catalysts. An Enraf Nonius FR590 sealed tube diffractometer, with a monochromatic Cu Kα1 source operated at 40 kV and 30 mA was used. Unit cell parameters were refined using the program FullProf [22].

Raman spectra were recorded at ambient temperature with a 514 nm laser excitation on a Renishaw Raman Spectrometer ("in via") equipped with a CCD detector. The laser power on the sample was 25 mW and a total of 20 acquisitions were taken for each spectra.

X-ray photoelectron spectroscopy (XPS) measurements were performed on a SPECS spectrometer with a MCD-9 detector and using a non monochromatic Al Kα (1486.6 eV) X-ray source. Spectra were recorded using an analyzer pass energy of 50 V, an X-ray power of 200 W and under an operating pressure of 10^{-9} mbar. Spectra treatment has been performed using the CASA software. Binding energies (BE) were referenced to the Ce3dv_1 peak at 882.17 eV.

Oxygen isotopic-exchange experiments were conducted using a quartz microreactor coupled to a quadrupole mass spectrometer (Omnistar, QMG 220 M1). Before each experiment the catalyst was initially pretreated at 450 °C for 2.5 h (in 50% $^{16}O_2$/Ar; flow 36 ml min^{-1}), followed by cooling down to 150 °C. Once achieved 150 °C, oxygen was replaced by argon (20 ml min^{-1}) and keep 1.5 h at that temperature before cooling down to 25 °C. For the temperature programmed isotopic exchange experiments (TPIE), the catalyst (0.160 g) was subjected to a 10% $^{18}O_2$/Ar flow (22 ml min^{-1}) and the temperature was raised from 25 to 650 °C (heating rate of 10 °C min^{-1}). The concentration profiles of the exit gas composition were obtained by acquiring the mass spectra signals relative to $^{18}O_2$ (m/e = 36), $^{16}O^{18}O$ (m/e = 34) and $^{16}O_2$ (m/e = 32). Blank run experiments were performed using an empty reactor in order to check contributions of the gas-phase reactions, and stability of the mass spectrometer.

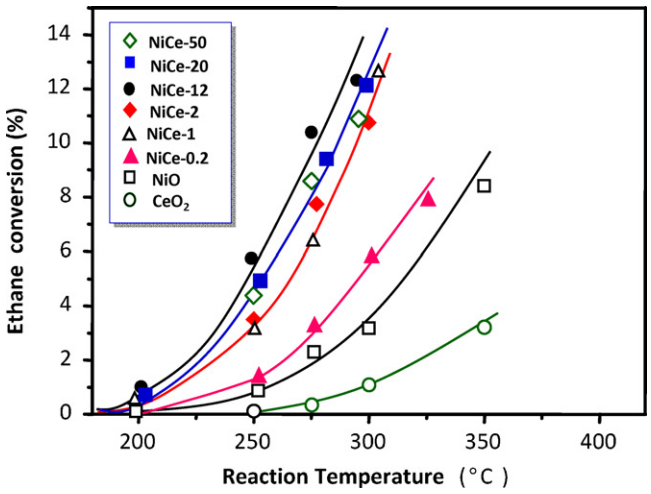

Fig. 1. Variation of the ethane conversion with the reaction temperature for some representative catalysts. Contact time, *W*/*F*, of 80 g_{cat} h/mol-C_2. Catalysts: NiO (□); NiCe-50 (◇); NiCe-20 (■); NiCe-12 (●); NiCe-2 (◆); NiCe-1 (△); NiCe-0.2 (▲); CeO_2 (○). (For interpretation of the references to color in this figure legend, the reader is referred to the web version of the article.)

The FTIR spectra were collected with a FTS-40A BioRad spectrometer equipped with a DTGS detector (4 cm^{-1} resolution, 32 scans). An IR cell allowing in situ treatments in controlled atmospheres and temperatures from −176 °C to 500 °C has been connected to a vacuum system with gas dosing facility. Self-supporting pellets (ca. 10 mg cm^{-2}) were prepared from the sample powders and treated at 250 °C in oxygen flow (20 ml min^{-1}) for 1.5 h followed by evacuation at 10^{-4} mbar at the same temperature for 1 h. After activation the samples were cooled down to −176 °C under dynamic vacuum conditions followed by CO dosing at increasing pressure (0.04–8.5 mbar). IR spectra were recorded after each dosage.

Temperature-programmed reduction (H_2-TPR) was carried out in a Micromeritics Autochem 2910 equipped with a TCD detector. The reducing gas used in all experiments was 10% H_2 in Ar, with a flow rate of 50 ml min^{-1}. The temperature range explored was from room temperature to 600 °C, and the heating rate was maintained at 10 °C min^{-1}.

2.3. Catalytic tests

The catalytic experiments were carried out at atmospheric pressure, in the 200–350 °C temperature range, using a fixed bed quartz tubular reactor (i.d., 20 mm, length, 400 mm). The feed consisted in a mixture of C_2H_6/O_2/He with molar ratios of 9.1/3/87.9. The catalyst amounts loaded and the total flows used were largely varied to achieve different conversions at a given temperature. Typical reaction conditions used were 0.5 g of catalyst and 25 ml/min. Catalyst samples were introduced in the reactor diluted with silicon carbide in order to keep a constant volume in the catalytic bed. Reactant and products were analyzed by gas chromatography using two packed columns: (i) molecular sieve 5 Å (2.5 m); and (ii) Porapak Q (3 m). Blank runs showed no conversion in the range of reaction temperatures employed.

3. Results and discussion

3.1. Oxidative dehydrogenation of ethane over Ni–Ce–O mixed metal oxides

Fig. 1 shows the variation of the ethane conversion with the reaction temperature for several representative Ni–Ce–O catalysts,

Table 1
Physico-chemical properties of Ce–Ni–O catalysts.

Catalyst	Ni/Ce at. ratio	Ethane conversion (%)[a]	Selectivity to ethylene (%)[a]	Catalytic activity		STY ($g_{C_2H_4}$ kg_{cat}^{-1} h^{-1})[d]
				($g_{C_2H_6}$ kg_{Ni}^{-1} h^{-1})[b]	(10^{-5} $g_{C_2H_6}$ m^{-2} h^{-1})[c]	
NiO	∞	2.3	39.9	10.7	54.7	3.14
NiCe-50	50	8.6	57.6	41.8	49.7	16.9
NiCe-20	20	9.4	59.2	48.4	48.1	19.0
NiCe-12	12	10.4	59.0	56.9	45.6	21.0
NiCe-6	6	9.5	60.2	59.7	n.d.	19.6
NiCe-3	3	7.9	64.8	62.5	36.6	17.5
NiCe-2	2	7.8	64.2	74.3	37.8	17.1
NiCe-1	1	6.7	60.0	96.5	38.2	13.7
NiCe-0.5	0.5	4.9	63.4	118	n.d.	10.6
NiCe-0.2	0.2	2.8	54.0	174	n.d.	5.17
CeO_2	0	0.3	9.1	–	2.67	0.09

[a] The catalytic results were achieved at $W/F = 80\ g_{cat}^{-1}\ h\ (mol_{C_2H_6})^{-1}$; reaction temperature = 275 °C, remaining reaction conditions in text.
[b] Catalytic activity per kg of nickel in the catalyst, in $g_{C_2H_6}\ kg_{Ni}^{-1}\ h^{-1}$.
[c] Specific activity (catalytic activity normalized per surface area), in $10^{-5}\ g_{C_2H_6}\ m^{-2}\ h^{-1}$.
[d] Rate of formation of ethylene per unit mass of catalysts, STY, in $g_{C_2H_4}\ kg_{cat}^{-1}\ h^{-1}$.

while Table 1 shows comparatively the composition and catalytic behaviour of all the catalysts studied. Independently of the Ni/Ce ratio, mixed Ni–Ce–O catalysts are considerably more active than pure NiO or pure CeO_2. In addition, we can inform that these mixed oxide catalysts are very active since appreciable activity has been obtained at only 250 °C.

Fig. 2 presents the variation of the selectivity to ethylene with the ethane conversion at 300 °C. It can be observed that all catalysts present an almost flat trend, hardly decreasing the selectivity to ethylene with the ethane conversion, suggesting that ethylene in the conversions range studied is very stable and almost do not decompose into carbon oxides. There are some previous works which, similarly to the present article, show scarce ethylene decomposition for pure NiO or for doped NiO catalysts (Ni–Nb–O, Ni–W–O, Ni–Ga–O, Ni–Al–O, Ni–Mg–O, . . .) [7–9,11,12].

CeO_2 is the least selective catalyst (ca. 8%) meanwhile NiO presents an intermediate value (ca. 40%). Mixed Ni–Ce–O catalysts resulted to be the most selective ones with selectivity to ethylene ranging from 60 to 65%. We must indicate that these mixed catalysts present a relatively stable performance since after 9 h on line no apparent variation in either conversion or selectivity to ethylene has been observed.

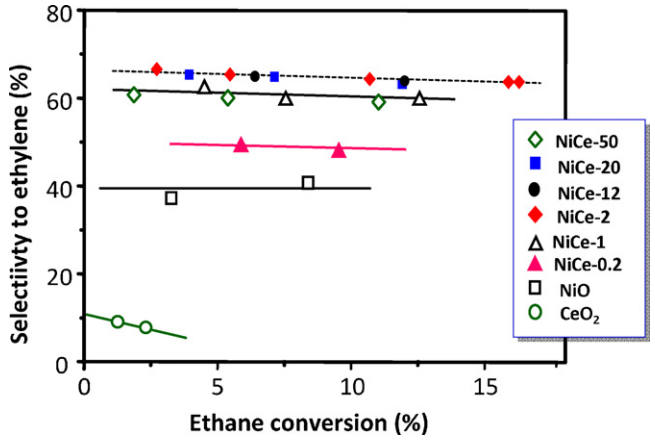

Fig. 2. Variation of the selectivity to ethylene with the ethane conversion for some representative catalysts. Reaction conditions: temperature = 300 °C and variable contact times. Catalysts: NiO (□); NiCe-50 (◇); NiCe-20 (■); NiCe-12 (●); NiCe-2 (◆); NiCe-1 (△); NiCe-0.2 (▲); CeO_2 (○). (For interpretation of the references to color in this figure legend, the reader is referred to the web version of the article.)

Since both the catalytic activity and the selectivity to ethylene are highest in Ni–Ce–O catalysts, the productivity to ethylene obtained over these mixed oxide catalysts will be much higher than that obtained over pure oxides, although the catalytic behaviour depends on the composition of the catalysts (Table 1). Those with Ni/Ce atomic ratios between 6 and 12 present the highest productivity. It is noteworthy that the incorporation of only a tiny amount of CeO_2 to NiO (i.e. Ni/Ce atomic ratio of 50) multiplies by 5 the productivity to ethylene. The increased activity of mixed oxides compared to pure NiO can be likely related to the increase of the surface area that occurs when CeO_2 is incorporated (Table 2) but also it could be related to other factors such as the change in the nature of Ni sites and/or even the catalytic contribution of Ce^{4+} sites (or CeO_2).

3.2. Characterization of Ni–Ce–O mixed oxides catalysts

Table 2 presents the main characteristics of Ni–Ce–O catalysts. It can be seen that the surface area of the catalysts strongly depends on the catalyst composition, the mixed oxides presenting in all cases higher surface areas than pure metal oxides.

Fig. 3 shows the XRD patterns of Ni–Ce–O catalysts. Two crystalline phases, i.e. NiO (JCPDS: 78-0643) and CeO_2 (JCPDS: 43-1002) are only observed, although the ratio between both phases strongly depends on the Ni/Ce ratio. On the other hand, the values of lattice parameters *c* for pure NiO, i.e. 4.173 Å, correspond in all cases to the ideal cubic cell [23]. However no apparent changes in the lattice parameters of NiO is observed in Ce-containing catalysts suggesting that a partial replacement of Ni^{2+} by Ce^{4+} in the framework of NiO does not take place.

In contrast with NiO, some differences in the lattice parameter of CeO_2 are observed for mixed Ni–Ce–O catalysts. In fact, the lattice parameters of CeO_2 decrease when increasing the Ni-content, which could indicate a partial replacement of Ce^{4+} by Ni^{2+} in the framework of CeO_2. This behaviour, with the probable formation of $Ce_{1-x}Ni_xO_2$, has been observed for catalysts with similar composition, although the amount of Ni incorporated could depend on the catalyst preparation procedure and catalyst calcinations [24].

What is clearly observed is the widening of the NiO and CeO_2 diffraction peaks for Ni–Ce–O catalysts if compared to pure catalysts. These wider bands mean smaller crystallite sizes in mixed catalysts, which fit with the higher surface areas observed. This decrease in the crystal size of NiO (from 35 to 9–12 nm) is observed for all mixed catalysts prepared even in that with a Ni/Ce atomic ratio of 50 (Table 2).

Table 2
Ce–Ni–O catalysts for the oxidative dehydrogenation of ethane to ethylene.

Catalyst	Ni/Ce at. ratio	Ni/(Ni + Ce) at. ratio (%)	S_{BET} (m^2/g)	NiO crystal size (nm)[a]	CeO_2 crystal size (nm)[a]	NiO lattice constant (Å)[b]	CeO_2 lattice constant (Å)[b]
NiO	∞	100	15.4	35.1	–	4.173	–
NiCe-50	50	98.0	63.4	12.1	n.d.	4.172	–
NiCe-20	20	95.2	71.6	10.8	n.d.	4.173	–
NiCe-12	12	92.3	83.5	9.7	9.3	4.173	–
NiCe-6	6	85.7	n.d.	10.1	9.3	4.174	–
NiCe-3	3	75.0	79.1	9.6	10.5	4.173	5.380
NiCe-2	2	66.7	75.5	10.0	10.7	4.173	5.349
NiCe-1	1	50.0	64.2	10.5	12.7	4.173	5.401
NiCe-0.5	0.5	33.3	n.d.	9.6	12.3	n.d.	5.403
NiCe-0.2	0.2	14.3	n.d.	n.d.	9.6	n.d.	5.408
CeO_2	0	0	14.1	–	13.5	–	5.409

[a] Crystal size estimated by the XRD patterns using the Scherrer equation.
[b] Lattice Constant of main crystalline phases, in Å.

Fig. 4 shows the Raman spectra of catalysts. The absorption peak at around 466 cm^{-1}, attributed to the F2g Raman active mode of fluorite structure in CeO_2 [25] is clearly observed at high Ce-contents. At lower ceria loadings, this peak is observed at 456 cm^{-1}, slightly shifted to lower frequencies probably due to same isomorphous substitution of Ni^{2+} into the CeO lattice [21]. In the case of samples with high Ni-loadings (from NiCe-12 to NiCe-50) the peak associated to CeO_2 is not observed, probably due to overlapping with absorption bands of NiO.

Pure NiO shows the absorption bands at 500 cm^{-1} with a shoulder at 410 cm^{-1} which are related to the Ni–O stretching mode in NiO [9,10,26]. As expected, the intensity of both bands decreases and the band at 500 cm^{-1} shifts to 516 cm^{-1} when the ceria loading increases.

The Ni2p3/2 XPS spectra of the Ni–Ce–O samples with different Ni/Ce atomic ratios and the reference NiO sample are shown in Fig. 5, while in Table 3 are summarized some of the XPS results. The

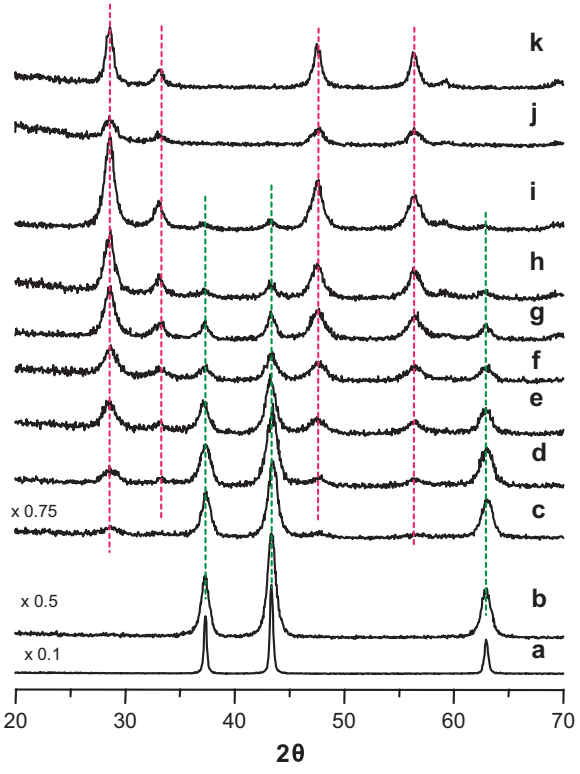

Fig. 3. XRD patterns of Ni–Ce–O mixed catalysts: (a) NiO; (b) NiCe-50; (c) NiCe-20; (d) NiCe-12; (e) NiCe-6; (f) NiCe-3; (g) NiCe-2; (h) NiCe-1; (i) NiCe-0.5; (j) NiCe-0.2; (k) CeO_2.

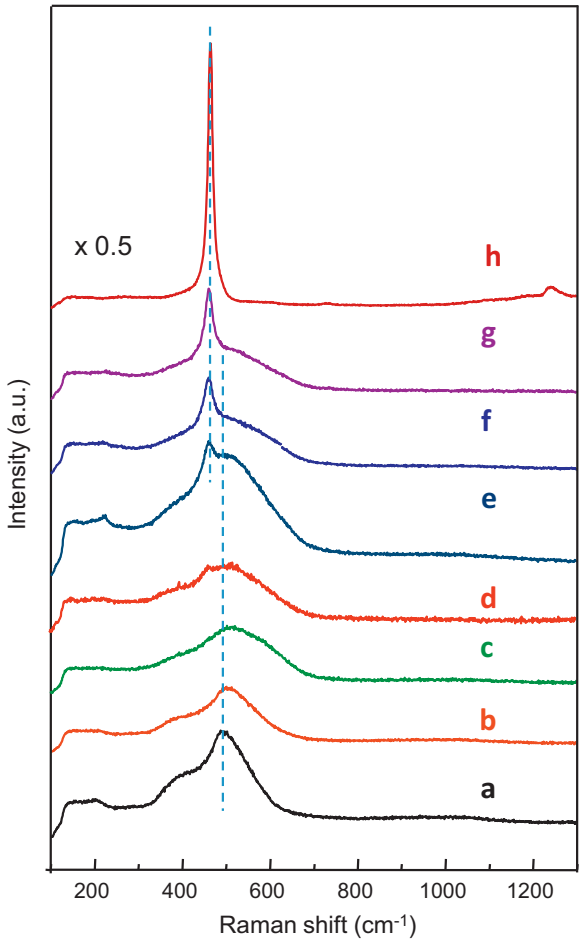

Fig. 4. Raman spectra of Ni–Ce–O catalysts: (a) NiO; (b) NiCe-50; (c) NiCe-20; (d) NiCe-12; (e) NiCe-3; (f) NiCe-2; (g) NiCe-1; (h) CeO_2.

Table 3
XPS of Ni–Ce–O mixed oxides catalysts.

Sample	Ni2p3/2 (BE)				Ni/Ce at. ratio	
	A (eV)	B (eV)	B/A (%)	Sat/main	Surface	Bulk[a]
NiO	853.74	855.42	3.55	3.16	–	–
NiCe-12	853.87	855.57	5.29	4.36	25	12
NiCe-3	853.45	855.15	3.94	3.76	4.5	3
NiCe-1	853.54	855.54	0.93	0.83	1.4	1

[a] From ICP analysis.

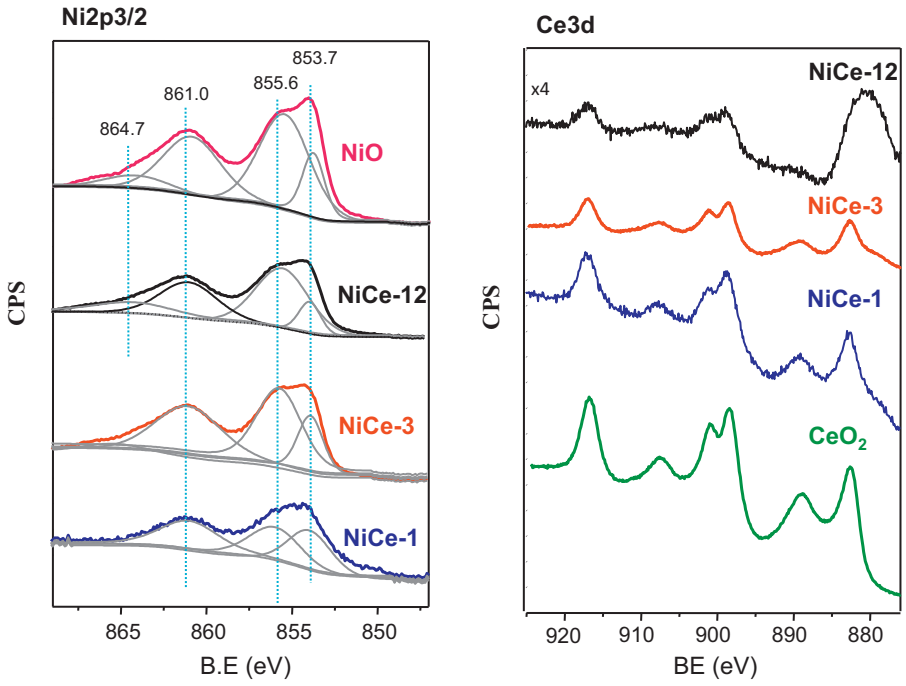

Fig. 5. X-ray photoelectron spectra of Ni2p3/2 and Ce3d of Ni–Ce–O mixed oxides catalysts. Catalyst composition as in Table 1.

Ni2p3/2 XPS line shows two well resolved components at BE 853.7 and 855.6 eV, and shake-up satellites at 861.0 and 864.7 eV. According to the literature, the high BE component has been assigned to Ni^{3+} ions [27,28], Ni^{2+}–OH species [29], or due to lattice distortions induced by the presence of Ni^{2+} vacancies [30,31]. Data of Table 3 shows a high amount of this type of site (labelled as site B) versus the Ni^{2+} surface site of BE 853.7 eV (labelled as site A) in particular in the NiCe-12 sample. On the other hand, the relative intensity of the satellite peaks at around 861.0 eV versus the Ni^{2+} main peak at 853.7 eV is higher in the NiCe-12 sample. This satellite peak is very sensitive on the structure arrangement and the nature of the Ni^{2+} surrounding atoms. A completely different satellite–main peak ratio and a different intensity ratio of the two components at low and high BE is however observed in the NiCe-1 sample. Thus, the XPS results suggest a proportion of Ni^{2+} defects in the NiCe-12 samples higher than those achieved in pure NiO. On the other hand, a lower amount of defects and a different structure arrangement of the Ni^{2+} ions are observed in the NiCe-1 sample.

Fig. 5 shows also the Ce3d XPS spectra of some representative catalysts. In all cases Ce^{4+} is mainly observed, showing a complex spectra and reflecting hybridization between the Ce4f and O2p states [32].

Finally, the surface composition of the samples is given in Table 3. It can be seen in all cases that the Ni/Ce ratio on the catalysts surface is higher than those achieved for the bulk of catalysts.

Temperature programmed $^{18}O_2$ isotopic exchange measurements (TPIE) have been performed on NiCe-1 and NiCe-12 samples (with high and low ceria content, respectively (Fig. 6)). For comparison, the TPIE results obtained on pure NiO is also included (Fig. 6), in order to study the nature of oxygen species participating in the oxidative dehydrogenation reaction of ethane to ethylene.

The oxygen exchange process commences at lower temperature on the ceria containing samples (204 and 215 °C on NiCe-1 and NiCe-12, respectively) compared to the higher temperature observed on NiO sample (345 °C) (Fig. 6). This behaviour indicates an increase in the mobility of oxygen species in Ce-containing catalysts. Thus, in Ce-rich catalysts, the presence of ceria could have an opposite effect to that observed on Nb-containing NiO catalysts [9], in which the incorporation of Nb^{5+} decreases the mobility of oxygen species.

On the other hand, a different distribution of isotopic oxygen species is observed on the ceria containing NiO samples, depending on the ceria content (Fig. 6). At high ceria content (sample NiCe-1) the amount of both the doubly exchanged $^{16}O_2$ species and the cross-labelled $^{16}O^{18}O$ species are high, being prevalent the formation of $^{16}O_2$, indicating a fast incorporation and diffusion of oxygen species into the bulk of the catalyst.

In samples with lower ceria content (i.e. NiCe-12 sample), the amount of double exchanged $^{16}O^{18}O$ is higher than that of $^{16}O_2$ (Fig. 6), indicating that oxygen dissociation is faster than their diffusion into the bulk. The oxygen diffusion into the bulk was lower than that in the NiCe-1 sample. However, the oxygen diffusion into the bulk is still enhanced compared to the Ce-free NiO catalysts, where the oxygen diffusion into the bulk decreases (enhancing the concentration of active electrophilic species on the catalysts surface). Accordingly, the presence of ceria in the NiO catalysts increases the diffusion of oxygen in the bulk, which under catalytic conditions could facilitate a fast reoxidation of the catalyst.

Fig. 7 shows the infrared spectra of CO adsorbed on Ni–Ce–O catalysts. These experiments have been conducted using a low dose of CO (ca. 0.05–0.10 mbar) in order to avoid the interaction of CO with the hydroxyl groups of the catalysts. As observed from the IR spectra, the nature of Lewis acid sites depends on the catalyst composition (i.e. ceria content).

Pure CeO_2 shows different Lewis acid sites (characterized by IR bands of adsorbed CO at 2176, 2161, 2150 (related to Ce^{4+} with different acidity); and 2123 cm^{-1} (related to Ce^{3+}) [33]. In the presence of nickel the more acidic Lewis surface sites (IR band at 2176 cm^{-1}) strongly decreases while less acid surface sites (IR bands at 2161 and 2150 cm^{-1}) starts to predominate. Indeed one band at 2150 cm^{-1} is mainly observed in the NiCe-12 sample. At this point, it is interesting to notice the absence of Lewis acid sites in pure NiO sample. Thus, we can infer that the presence of ceria increases the amount of unsaturated surface sites, acting these as weak Lewis acid sites. Ce^{3+} species (IR band at 2123 cm^{-1}) are on the other hand, observed in very low amount in all samples.

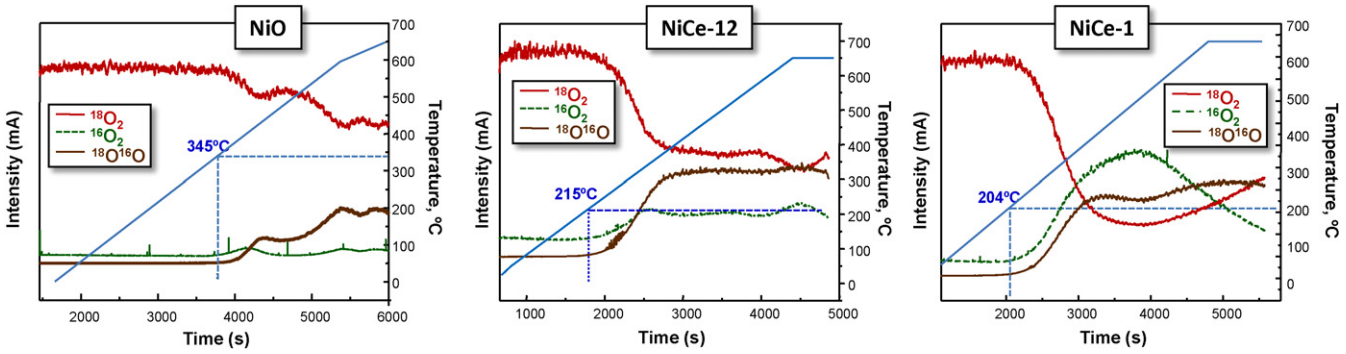

Fig. 6. Temperature programmed $^{18}O_2$ isotopic oxygen exchange profiles of NiO, NiCe-12, and NiCe-1.

Fig. 8 shows the H_2-TPR profiles of Ce–Ni–O catalysts. Pure NiO catalyst presents a main reduction with two maxima at 285 °C and 310 °C. This profile is consistent with the reduction of two types of Ni^{2+} (or Ni^{3+}) species to metallic nickel [34,35]. These two reduction peaks are also observed when cerium is present in low amounts (i.e., NiCe-50, NiCe-20 and NiCe-12 catalysts). However, the low temperature peak decreases and the high temperature peak increases when increasing the Ce-content. In addition, the peak at high temperature shifts towards higher reduction temperatures when the cerium loading increases. This indicates that small amounts of cerium modify the nature of the Ni-species and this can be related to the improvement in the catalytic performance of these catalysts.

A different behaviour is observed in samples with $1 < Ce/Ni < 6$ ratios. In these cases, it is observed preferentially three reduction peaks at 205, 265 and 310–340 °C. The reduction peak at 205 °C is associated to the reduction of adsorbed oxygen species in CeO_2 [21,24,36]. However, the reduction temperature at 265 and 310–340 °C should be related to reduction of Ni^{2+} species. At this point, it is interesting to indicate that, in agreement to XRD and Raman, Ni^{2+} species can be incorporated partially into CeO_2, in addition to the formation of NiO. However, at this moment it is difficult to quantify the amount of Ni^{2+} species in each crystalline phase.

On the other hand, the involvement of cerium species in the TPR profiles of these Ce-rich catalysts cannot be ruled out. However if present they would be of low intensity, as pure CeO_2 in the temperature range studied shows only a wide but low intensity reduction. Moreover these reductions of the Ce-species would be likely overlapped by the more intense Ni-species bands. In fact, the H_2-uptake related to the reduction peaks in the 250–450 °C in catalysts decreases when decreasing the Ni-content. Thus the H_2-uptake for NiO, NiCe-12 and NiCe-1 catalysts is 382.4, 329.1 and 128.1 mL g^{-1}, respectively. Since, the amount of H_2 involved

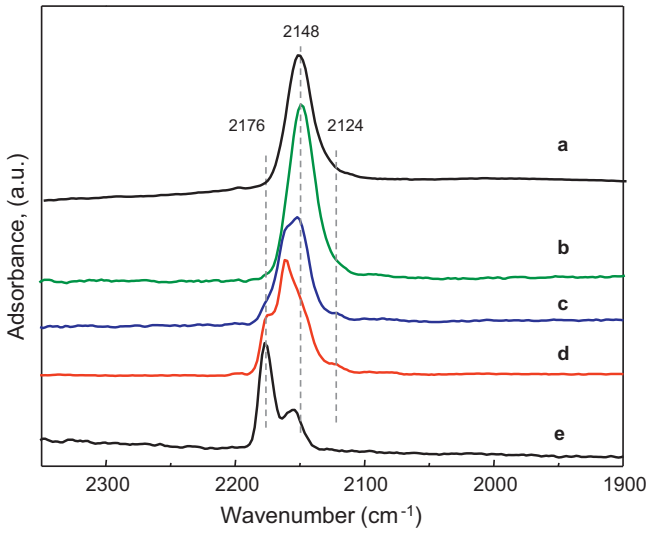

Fig. 7. FTIR spectra at −176 °C of Ni–Ce–O catalysts after CO adsorption (0.05–0.10 mbar). Catalysts: (a) NiO; (b) NiCe-12; (c) NiCe-3; (d) NiCe-1; (e) CeO_2.

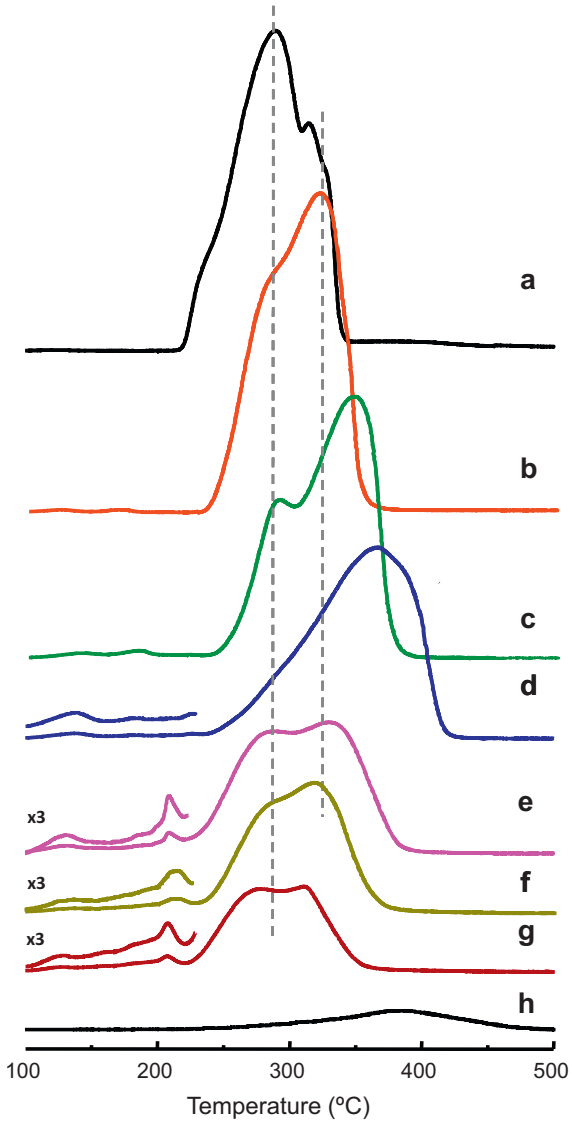

Fig. 8. H_2-TPR patterns of Ni–Ce–O catalysts: (a) NiO; (b) NiCe-50; (c) NiCe-20; (d) NiCe-12; (e) NiCe-3; (f) NiCe-2; (g) NiCe-1; (h) CeO_2.

in these three cases corresponds to ca. 0.0018 mol_{H_2} g_{Ni}, it can be concluded that, in all cases, NiO is completely reduced.

Pure CeO_2 presents a small broad peak until 500 °C, centred at 380 °C, which can be attributed to surface reduction of surface oxygen species [37–40]. It must be noted that the reduction of the bulk of CeO_2 does not take place in the interval of temperature studied, since this usually occurs above 700 °C [37–40].

3.3. On the influence of chemical composition of catalyst on catalytic behaviour

Ni–Ce–O mixed oxides catalysts are more active and selective in the ODH of ethane than pure NiO. Thus, for the optimal Ni–Ce–O catalyst, a productivity to ethylene of ca. 7 times higher than pure NiO has been observed. However, and although Ni-sites are the active sites for ODH, high differences in catalytic activity are not observed for catalysts with Ni/(Ni + Ce) content from 95 to 70%. This performance could be explained by considering redox properties, i.e. reducibility (determined by H_2-TPR) and reoxidation capability (determined by TPIE). In this way, reducibility decreases as: NiO > NiCe-1 > NiCe-12; whereas reoxidation capability decreases as: NiCe-1 > NiCe-12 > NiO. In other words, the catalytic activity will be directly related to the rate of H-abstraction (which depends on the catalyst reducibility) but also with the rate of reoxidation of active sites (which depend on the bulk oxygen mobility) in a Mars van-Krevelen mechanism.

On the other hand, and according to both the catalytic and the characterization results two different types of catalysts can be proposed: (i) CeO_2-promoted NiO catalysts, at Ni/Ce content higher than 6, in which the presence of ceria promote the formation of NiO particles with low crystal sizes; (ii) CeO_2–NiO mixed oxides, observed at Ni/Ce ratios lower than 6, in which it can be proposed the presence of NiO, CeO_2 and a probable partial incorporation of Ni^{2+} into ceria (i.e. with the formation of $Ce_{1-x}Ni_xO_2$).

Apparently the incorporation of Ce^{4+} to NiO is not produced in our catalysts. However, Ni^{2+} seems to be incorporated to a certain extent into the ceria lattice for catalysts with high Ce-contents. This is in agreement with previous works which propose that the incorporation of Ni^{2+} seems to be more favoured than the incorporation of Ce^{4+} into nickel oxide lattice [24], due to the fact that the radius of Ni^{2+} (0.72 Å) is lower than that of Ce^{4+} (1.01 Å). Thus, and according to our XRD and Raman results, it can be concluded that both NiO and Ni-free and Ni-containing CeO_2 (as $Ce_{1-x}Ni_xO$) could coexist in mixed Ni–Ce–O catalysts, this being more relevant for samples with Ni/Ce atomic ratios between 1 and 12.

Changes in the nature of the crystalline phases can be also proposed from the TPR experiments. Thus, the TPR results of CeO_2-promoted NiO show that the reducibility of Ni-species initially decreases when increasing the Ce-content (at the same time the reduction peak shifts to higher temperatures when increasing the Ce-content). The higher selectivity to ethylene observed in these catalysts could be related to a partial decrease of high reducible Ni-sites (probably involved in ethane combustion) and a higher formation of less-reducible Ni-sites (probably involved in the ODH of ethane). A similar behaviour has been observed in Nb-promoted NiO catalysts [9].

However, catalysts with Ni/Ce atomic ratios lower than 6 show important changes in their H_2-TPR patterns. Thus, the reducibility of Ni-species is higher than that observed for NiCe-12 sample, and seems to be similar to that observed for pure NiO (the temperature of the maximum in the reduction peaks is similar to that of NiO). This result could be explained by considering the presence of NiO and Ni-containing CeO_2 (i.e. $Ce_{1-x}Ni_xO_2$, proposed by Li et al. [24]), with relatively low crystal size, which could facilitate a synergic effect between both phases. This is also suggested by temperature programmed $^{18}O_2$ isotopic exchange measurements (TPIE) in which the mobility of oxygen species in Ce-rich samples is higher than that observed in Ce-poor samples, which is also higher than that observed for NiO. Accordingly, the improvement of catalytic activity for ethane oxidation and selectivity to ethylene in Ce-rich NiO catalysts could be explained by considering that Ce-rich Ni–Ce–O catalysts present high reducibility and high oxygen mobility, which could facilitate not only a rapid ethane oxidation but also a rapid reoxidation of active sites.

On the other hand, the presence of ceria increases in some way the amount of unsaturated surface sites, acting these as weak Lewis acid sites. Since, it has been proposed that the presence of Lewis acid sites can facilitate ethylene desorption during the ODH of ethane, the presence of an excess of CeO_2 could promote a fast reoxidation of the active Ni-sites (CeO_2 can favour a higher concentration of O^{2-} species on the catalyst surface), facilitating also a fast desorption of ethylene (by increasing the concentration of Lewis acid sites on the catalyst surface).

The temperature programmed $^{18}O_2$ isotope-exchange technique (TPIE) helps us in determining the nature of the oxygen species acting in the reaction mechanism. Thus, the distribution of isotopic exchange products ($^{16}O_2$ and $^{16}O^{18}O$) depends on the relative rates of oxygen dissociation, surface exchange process, lattice incorporation and diffusion into the bulk [8]. A fast oxygen dissociation followed by a rapid surface oxygen exchange process compared with the oxygen diffusion rate into the bulk leads to the formation of $^{16}O^{18}O$, while a faster incorporation reaction and subsequent diffusion step into the bulk results in $^{16}O_2$ as the dominant product [41]. Considering that the oxidative dehydrogenation of ethane on NiO based catalysts takes place by a redox mechanism meanwhile the oxidation of ethane to CO_2 mainly through a surface mechanism [8], $^{16}O_2$ species should be mainly detected in TPIE experiments with catalysts selective to ethylene, meanwhile $^{16}O^{18}O$ in catalysts selective to CO_2. Accordingly, in the present work it is observed that cerium containing catalysts present a $^{16}O_2/^{16}O^{18}O$ ratio higher than pure NiO, which can justify the higher selectivity to ethylene observed for Ce-containing NiO catalysts.

4. Conclusions

Ni–Ce–O mixed metal oxides catalysts have been found to be active and selective in the oxidative dehydrogenation of ethane, at low reaction temperature. These catalysts can activate ethane at temperatures even below 250 °C obtaining selectivities towards ethylene of 60–65%. Interestingly, the selectivity to ethylene hardly varies in the range of conversions studied, suggesting that the ethylene formed does not (or almost does not) decompose into carbon oxides.

The addition of only a tiny amount of cerium (Ni/Ce = 50 at. ratio) to NiO leads to an increase in the catalytic activity which has been related to the increase in the surface area and the higher oxygen mobility that occurs if cerium is present in the catalysts. This enhanced activity is maintained and even exceeded for the different cerium contents studied.

The selectivity to ethylene is also higher in mixed Ni–Ce–O catalysts than in pure NiO. This higher selectivity has been related to the a faster diffusion of oxygen into the bulk and a lower amount of oxidizing surface oxygen species in mixed catalysts compared to pure NiO, thus decreasing the formation of carbon dioxide.

On the other hand, the catalytic activity per Ni site and surface area increases when increasing the Ce-content. In this case, it is observed the presence of NiO and CeO_2, but also a partial incorporation of Ni^{2+} into CeO_2, i.e. the partial formation of $Ce_{1-x}Ni_xO_2$ phase, in addition to CeO_2 and NiO. These catalysts show Lewis acid sites on the catalyst surface (the amount of acid sites is lower than

those observed in pure CeO_2 but higher than those observed on NiO or Ce-doped NiO catalysts) as well as a reducibility of Ni-sites (and a mobility of oxygen species) higher than those achieved over Ce-poor NiO samples.

The catalytic activity has been shown to depend on the Ni/Ce ratio. The rate of formation of ethylene per unit mass of catalyst was highest over NiCe-12 catalyst ($21.0\,g_{C_2H_4}\,kg_{cat}^{-1}\,h^{-1}$ at only 275 °C, which is ca. 7 times higher than that achieved by pure NiO).

Acknowledgements

The authors would like to thank the DGICYT in Spain (Project CTQ2009-14495) for financial support. SH thanks a fellowship from DGICYT.

References

[1] F. Cavani, F. Trifiró, Catal. Today 51 (1999) 561–580.
[2] M.M. Bhasin, Top. Catal. 23 (2003) 145–149.
[3] D.N. Nakamura, Oil Gas J. 107 (2009) 43–54.
[4] T. Ren, M.K. Patel, K. Blok, Energy 33 (2008) 817–833.
[5] J.M. López Nieto, P. Botella, M.I. Vázquez, A. Dejoz, Chem. Commun. (2002) 1906–1907.
[6] P. Botella, E. García-González, A. Dejoz, J.M. López Nieto, M.I. Vázquez, J. González-Calbet, J. Catal. 225 (2004) 428–438.
[7] E. Heracleous, A.F. Lee, K. Wilson, A.A. Lemonidou, J. Catal. 231 (2005) 159–171.
[8] E. Heracleous, A.A. Lemonidou, J. Catal. 237 (2006) 175–189.
[9] E. Heracleous, A.A. Lemonidou, J. Catal. 237 (2006) 162–174.
[10] B. Savova, S. Loridant, D. Filkova, J.M.M. Millet, Appl. Catal. A 390 (2010) 148–157.
[11] B. Solsona, A.M. Dejoz, I. Vázquez, F. Ivars, J.M. López Nieto, Top. Catal. 52 (2009) 751–757.
[12] E. Heracleous, A.A. Lemonidou, J. Catal. 270 (2010) 67–75.
[13] X. Zhang, Y. Gong, G. Yu, Y. Xie, J. Mol. Catal. A: Chem. 180 (2002) 293–298.
[14] A. Kaddouri, R. Anouchinsky, C. Mazzocchia, L.M. Madeira, M.F. Portela, Catal. Today 40 (1998) 201–206.
[15] F. Cavani, N. Ballarini, A. Cericola, Catal. Today 127 (2007) 113–131.
[16] A. Trovarelli, M. Boaro, E. Rocchini, C. Leitenburg, G. Dolcetti, J. Alloys Compd. 323–324 (2001) 584–591.
[17] W. Liu, M. Flytzani-Stephanopoulos, J. Catal. 153 (1995) 304–316.
[18] H. Sakurai, A. Ueda, T. Kobayashi, M. Haruta, Chem. Commun. (1997) 271–272.
[19] L. Jalowiecki-Duhamel, A. Ponchel, C. Lamonier, A. D'Huysser, Y. Barbaux, Langmuir 17 (2001) 1511–1517.
[20] P. Boizumault-Moriceau, A. Pennequin, B. Grzybowska, Y. Barbaux, Appl. Catal. A: Gen. 245 (2003) 55–67.
[21] Y.M. Liu, L.C. Wang, M. Chen, J. Xu, Y. Cao, H.Y. He, K.N. Fan, Catal. Lett. 130 (2009) 350–354.
[22] J. Rodríguez-Carvajal, FullProf, Version 3.30, Laboratoire Léon Brillouin (LLB), 2005.
[23] E. Antolini, Mater. Lett. 51 (2001) 385–388.
[24] W. Shan, M. Luo, P. Ying, W. Shen, C. Li, Appl. Catal. A 246 (2003) 1–9.
[25] B.M. Reddy, A. Khan, P. Lakshmanan, M. Aouine, S. Loridant, J.C. Volta, J. Phys. Chem. B 109 (2005) 3355–3363.
[26] S.S. Chan, I.E. Wachs, J. Catal. 103 (1987) 224–227.
[27] M.J. Tomellini, J. Chem. Soc., Faraday Trans. 1 (84) (1988) 3501–3510.
[28] P. Salagre, J.L.G. Fierro, F. Medina, J.E. Sueiras, J. Mol. Catal. A 106 (1996) 125–134.
[29] J.C. Vedrine, G. Hollinger, T.M. Duc, J. Phys. Chem. 82 (1978) 1515–1520.
[30] V. Biju, M. AbduKhadar, J. Nanop. Res. 4 (2002) 247–253.
[31] D. Alders, F.C. Voogt, T. Hibma, G.A. Sawatzky, Phys. Rev. B 54 (1996) 7716–7719.
[32] J.P. Holgado, R. Alvarez, G. Munuera, Appl. Surf. Sci. 161 (2000) 301–315.
[33] Cl. Binet, M. Daturi, J.Cl. Lavalley, Catal. Today 50 (1999) 207–225.
[34] T. Takeguchi, S. Furukawa, M. Inoue, J. Catal. 202 (2001) 14–24.
[35] J.T. Richardson, B. Turk, M.V. Twigg, Appl. Catal. A 148 (1996) 97–112.
[36] N. Yisup, Y. Cao, W.-L. Feng, W.-L. Dai, K.-N. Fan, Catal. Lett. 99 (2005) 207–213.
[37] D. Andreeva, R. Nedyalkova, L. Ilieva, M.V. Abrashev, Appl. Catal. B 52 (2004) 157–165.
[38] G.W. Graham, W.H. Weber, C.R. Peters, R. Usmen, J. Catal. 130 (1991) 310–313.
[39] H.C. Yao, Y. Yu, J. Catal. 86 (1984) 254–265.
[40] M.F.L. Johnson, J. Mooi, J. Catal. 103 (1987) 502–505.
[41] J. Zhu, J.G. van Ommen, H.J.M. Bouwmeester, L. Lefferts, J. Catal. 233 (2005) 434–441.